2016

CFD Based Comparison of Slit Fin and Louver Fin Performance for Small Diameter (3mm to 5 mm) Heat Exchangers

Shekhar Sarpotdar
Optimized Thermal Systems, 7040 Virginia Manor Road, Beltsville, MD, 20705, sarpotdar@optimizedthermalsystems.com

Dennis Nasuta
Optimized Thermal Systems, 7040 Virginia Manor Road, Beltsville, MD, 20705, nasuta@optimizedthermalsystems.com

Vikrant Aute
vikrant@umd.edu

CFD Based Comparison of Slit Fin and Louver Fin Performance for Small Diameter (3mm to 5 mm) Heat Exchangers

Shekhar SARPOTDAR[1*], Dennis NASUTA[2], Vikrant AUTE[3]

[1,2,3]Optimized thermal Systems, Inc.
7040 Virginia Manor Road, Beltsville, MD, 20705
[3]Center for Environmental Energy Engineering
Department of Mechanical Engineering, University of Maryland
College Park, MD, 20742
Email: [1]sarpotdar@optimizedthermalsystems.com, [2]nasuta@optimizedthermalsystems.com, [3]vikrant@umd.edu
* Corresponding Author

ABSTRACT

Tube and fin heat exchangers using small diameter (≤5mm outer diameter (OD)) copper tubes are emerging as desirable alternatives to heat exchangers using conventional (≥7mm OD) tubes. Enhanced fins, having slits or louvers, have high heat transfer performance and are often used in tube and fin heat exchangers. Present literature lacks air side pressure drop and heat transfer coefficient correlations for these fin designs for tube diameters smaller than 5 mm. In this paper, the development of correlations for slits fins for tube diameters ranging from 3 mm to 5 mm. These correlations are developed following the Computational Fluid Dynamics (CFD) based methodology as outlined in the companion paper "CFD-Based Airside Heat Transfer and Pressure Drop Correlation Development for Small Diameter (3 mm to 5 mm) Copper Tube Louver Fin Heat Exchangers". The correlation for the Colburn *j* factor developed in this paper reproduces 93% of heat transfer data, obtained through CFD simulations, within 85% accuracy. The Darcy f factor correlation reproduces 98% of pressure drop data, obtained through CFD simulations, within 90% accuracy. Using these correlations, a comparative analysis for slit fin and louver fin performance is undertaken. Performance trends with respect to different fin design parameters such as the number of slits/ louvers, slit height, etc. are addressed. The work also includes an investigation of optimal fin design for each of the fin types. These correlations, and the optimal fin designs, can be used to design air-to-refrigerant heat exchangers with tube outer diameters between 3 and 5 mm.

1. INTRODUCTION

Researchers around the world are trying to optimize air-to-refrigerant heat exchangers with objectives such as maximizing heat transfer, minimizing power consumption, and minimizing the cost of the heat exchanger (Web & Kim 2005). Small tube diameter (OD < 5mm) heat exchangers are proving to be effective towards meeting these objectives (Paitoonsurikarn et al., 2000, Saji et al., 2001). However, the present literature lacks correlations that characterize the air-side pressure drop and Heat Transfer Coefficient (HTC) for tube diameters below 7 mm. In a companion paper "CFD-based airside heat transfer and pressure drop correlation development for small diameter (3 mm to 5 mm) louver fin heat exchangers" we presented CFD based correlations for louver fins for tube diameters ranging from 3 mm to 5 mm. In this paper we follow the same methodology and present correlations for slit fins ranging from 3 mm to 5 mm tube diameter. These correlations were then used to understand and compare the performance of slit and louver fins with respect to design parameters such as the number of slits, number of louvers etc. A multi-objective optimization study was also conducted to identify an optimized fin design that can be used by fin design manufacturers for an example scenario.

2. HEAT EXCHANGER MODELING AND DATA REDUCTION

To develop a new air-side correlation, seven topological features associated with the slit fin design were parameterized, as outlined in Table 1. Designs were limited to a staggered tube arrangement, as shown in the example engineering drawing depicted in Figure 1. Mochizuki et al. (1988) showed that reducing the ratio of slit height and slit

width (S_h/S_w) improves the performance of the slit fins. For tube diameters smaller than 5 mm, this would require a slit width smaller than 1 mm, which presents inherent manufacturing challenges. As such, the present study used a fixed S_w of 1 mm.

Table 1: Heat exchangers design space.

Design Variable	unit	Min to Max	Design Variable	unit	Min to Max
D_n	mm	3 to 5	FPI	--	14 to 40
D_c	mm	(1.023+0.1)+2 δ_f	$C_h=S_h/F_{Sp}$	--	0.3 to 0.7
$C_l = P_l/D_n$	--	2 to 4	S_w	mm	1
$C_t = P_t/P_l$	--	1.1 to 2	u	m/s	0.75 to 5
N	--	1 to 6	δ_f	mm	0.098

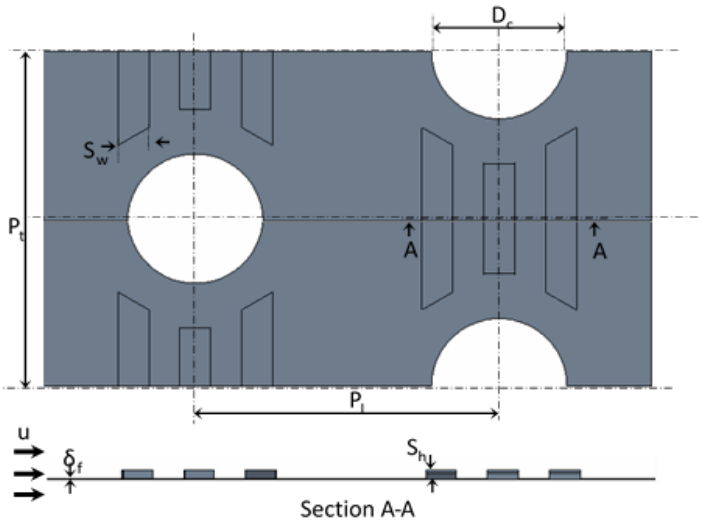

Figure 1: Slit fin design

The methodology used by Bacellar et al. (2014) was used for data reduction. The overall heat transfer coefficient (U) was calculated using Equations 1 and 2 as follows:

$$\dot{Q}=UA_o.\ LMTD \tag{1}$$

$$LMTD = \frac{(T_w-T_{air,in})-(T_w-T_{air,out})}{ln\left(\frac{T_w-T_{air,in}}{T_w-T_{airout}}\right)} \tag{2}$$

As mentioned by Bacellar et al. (2014), under the assumption that the thermal resistance associated with tube material and refrigerant boundary layer is negligible as compared to the air-side convective resistance, air-side HTC can be stated as:

$$h_{air}=\frac{U}{\eta_o} \tag{3}$$

Here the fin effectiveness (η_o) and consequently the fin efficiency (η), can be solved using Schmidt's (1949) fin efficiency formula. The Colburn j factor is determined based on maximum velocity ($u_{max} = u_{fr}/\sigma$) and is given by Equation 4.

$$j=\frac{h_{air}\,Pr^{\frac{2}{3}}}{\rho_m u_{max} c_{p_m}} \tag{4}$$

The friction factor is calculated based on the definition of Wang and Chi (2000), with the modification based on maximum velocity.

$$f = \frac{A_{min}}{A_o}\frac{\rho_m}{\rho_1}\left[\frac{2\Delta P \rho_1}{G_{max}^2}(1+\sigma^2)\left[\frac{\rho_1}{\rho_2}-1\right]\right] \quad (5)$$

Here the air side pressure drop is obtained from air mass-weighted average pressures at the inlet and outlet ($\Delta P = P_{in} - P_{out}$).

3. CFD MODELING

3.1 CFD Model

Table 1 lists all the design parameters with their respective ranges involved in the study. Using the two level full factorial method results in 256 design samples. An additional 1,000 designs were sampled using the latin hypercube technique. Care was taken to eliminate any infeasible designs before they were simulated. Boundary conditions included the tube wall temperature, which was set to 65ºC, and the inlet air temperature, which was set to 25ºC. The two-layer SST K-ω model was used for turbulence modeling. As mentioned earlier the present work is very similar to the one performed by Sarpotdar et al. (2016). Hence, here we present only important details of the CFD model, please refer to Sarpotdar et al. (2016) for additional details.

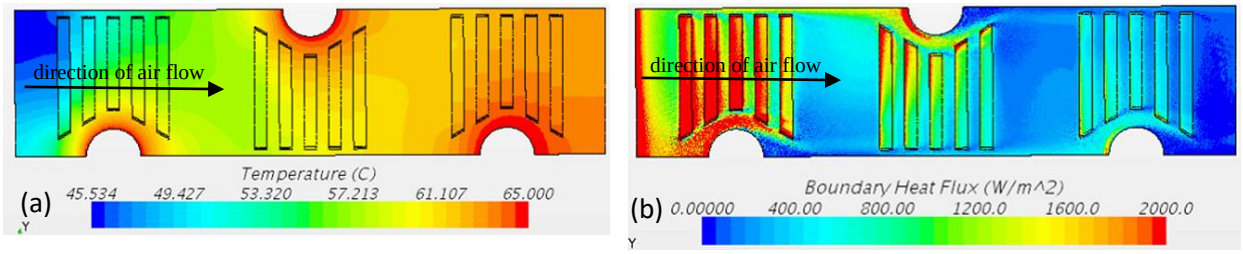

Figure 2: Sample CFD results. (a)Temperature contour plot; (b) heat flux contour plot

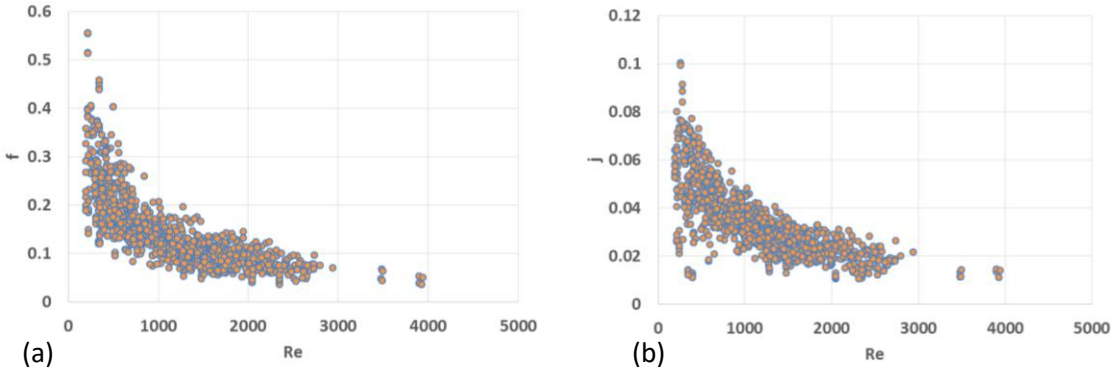

Figure 3: CFD results. (a) f factor; (b) j factor

A mesh independence study was performed following the Grid Convergence Index (GCI) criterion (Roach, 1997, ASME 2009). Each simulation was performed for three grid sizes, each with a successively finer grid having elements 1.35 times smaller than the previous grid. The study included a total of 1,032 simulations, but the mesh independence study was restricted to a limited number of cases on the boundaries of the design space. It was found that the mean uncertainty, due to the change in mesh size, was 1.7% and 1.3% in the pressure drop and HTC, respectively. This study confirmed that the selected mesh size was appropriate for the model.

Figure 3 shows sample CFD results for one of the cases. Figure 3a shows temperature contour plots, whereas figure 3b shows heat flux distribution on the fin surface. In Figure 3a one can see lower temperatures at the upstream edge of the fin. As one moves downstream and closer to the tube wall, the temperature of the fin increases. As indicated by the heat flux plot, the convective heat transfer between the air and the fin is higher at the upstream edge. Slits also show higher heat transfer values caused by boundary layer interruption and restarting. Figure 4 shows the results for

f and *j* factors for the entire sample space. Both *j* and *f* factor exhibit established trends with respect to Reynolds number, i.e., *f* and *j* factors decay exponentially as the Reynolds number increases.

3.2 Correlation Development

To characterize pressure drop and HTC, *f* and *j* correlations were developed using linear regression analysis. The generic form of the correlation is as shown in Equation 6.

$$ln(Z) = \sum ln(X_i)\, ln(Y_i)\, m_i \quad (6)$$

Here X_i and Y_i represent predictor terms such as P_l, Re, σ, etc. In the above equation m_i represents the coefficient in the i^{th} term. Z is the response variable such as *j* or *f*. Note that the *j* correlation was developed through an intermediate correlation for fin efficiency (η). Fin efficiency estimated through this correlation is referred to as $\eta_{estimator}$. Tables 2 ,3 and 4 list the individual terms for *f*, $\eta_{estimator}$, and *j*.

Table 5 gives a statistical summary of these correlations. The *f* correlation can predict 98.1 % of the CFD data within 90% accuracy. The *j* correlation can predict 84.7% of the CFD data within 90% accuracy. Figure 5 shows, in the form of a regression plot, how these correlations behave with respect to the CFD data

Table 2: *f* correlation

X,Y	m	X,Y	m	X,Y	m
2.7182, 2.7182	-41994991.24537	P_l,Re	-1472478.87830	N_s,φ	-0.08644
D_c,2.71828	36.77560	P_t,N	-21.66833	N_s,D_h	-0.17970
P_l,2.71828	-53048680.02234	P_t,S_h	10459673.27791	N_s,Re	0.04606
P_t,2.71828	-58768406.91082	P_t,N_s	2.02521	F_p,A_o	-21.42324
N,2.71828	-53048678.67123	P_t,F_p	-12750514.92639	F_p,D_h	-100.80694
S_h,2.71828	7250092.20989	P_t,A_{min}	-59.70876	A_{min},σ	-12750519.84166
N_s,2.71828	-0.87434	P_t,φ	-32.54775	A_{min},φ	5891175.29104
F_p,2.71828	-58768300.92739	P_t,Re	-1.04968	A_{min},Re	-1472477.54586
A_{min},2.71828	-3118345.71200	N,S_h	10459673.45764	A_o,φ	-5891142.54641
A_o,2.71828	53048663.62750	N,N_s	2.26581	A_o,D_h	12750594.48548
σ,2.71828	-67606333.80034	N,A_o	-12750561.97926	A_o,Re	1472478.26709
φ,2.71828	8166907.02225	N,σ	-21.25635	σ,φ	-19.48870
D_h,2.71828	53048629.06775	N,φ	5891142.50775	σ,D_h	-60.07573
Re,2.71828	-2041288.37187	N,D_h	-12750573.14933	σ,Re	-0.84615
D_c,F_p	37.78537	N,Re	-1472478.27938	φ,D_h	-5891173.13251
D_c,D_h	-34.49748	S_h,N_s	0.07868	φ,Re	0.58367
D_c,Re	0.72867	S_h,F_p	10459675.12781	D_h,Re	1472477.75159
P_l,N	12750562.92468	S_h,A_o	-10459673.43979	P_l,P_l	6375293.33505
P_l,S_h	10459673.38417	S_h,σ	10459673.53964	P_t,P_t	-6375231.61621
P_l,N_s	2.28334	S_h,D_h	-10459673.61392	N,N	6375270.12956
P_l,A_o	-12750584.63031	S_h,Re	0.04426	S_h,S_h	-0.67890
P_l,φ	5891142.04284	N_s,A_o	-2.27009	N_s,N_s	0.08410
P_l,D_h	-12750574.89155	N_s,σ	1.80827	F_p,F_p	-6375238.91309
σ,σ	6375246.50389	D_h,D_h	6375339.87789	Re,Re	0.06197
A_o,A_o	6375291.83074				

Table 3: Fin efficiency estimator correlation

X,Y	m	X,Y	m	X,Y	m
2.7182, 2.7182	17942179.39780	P_l,N_s	1305031.45923	N_s,φ	0.06476
D_c,2.71828	59.42796	P_l,A_o	2138113.92285	N_s,D_h	-1305032.45465
P_l,2.71828	24580093.93059	P_l,φ	-23.77095	N_s,Re	-0.01743
P_t,2.71828	27721182.25645	P_l,D_h	4276214.52988	F_p,A_o	-2138124.92949
N,2.71828	27544156.27186	P_l,Re	0.29166	F_p,φ	22.64856
S_h,2.71828	0.95186	P_t,N	4276183.58368	A_{min},σ	4276212.15951

N_s,2.71828	1809158.82066	P_t,S_h	-0.69534	A_{min},φ	-23.99134
F_p,2.71828	27721201.97545	P_t,F_p	4276214.44245	A_{min},Re	-0.97945
A_{min},2.71828	-177037.88059	P_t,A_o	-2138094.86315	A_o,σ	-2138126.06876
A_o,2.71828	-26062145.45095	P_t,Re	1.12838	A_o,D_h	-2138088.92362
σ,2.71828	30685238.11342	N,N_s	1305031.52996	σ,φ	23.05056
φ,2.71828	2.58317	N,F_p	4276213.85079	σ,D_h	7.04237
D_h,2.71828	-24580116.81677	N,A_o	-2138088.71037	σ,Re	0.48425
Re,2.71828	-2.07108	N,σ	4276214.82245	φ,Re	-0.42872
D_c,N	37.13123	N,φ	-0.00163	D_h,Re	1.05609
D_c,S_h	1.78204	N,Re	-0.02642	D_c,D_c	37.06197
D_c,F_p	48.26794	S_h,N_s	-0.01551	P_l,P_l	-2138104.79453
D_c,A_o	-37.08485	S_h,F_p	-0.43030	P_t,P_t	2138104.00230
D_c,σ	53.30460	S_h,σ	-0.97740	N,N	2138088.77009
D_c,φ	47.99006	S_h,φ	1.30097	S_h,S_h	0.25432
D_c,D_h	-50.09476	S_h,Re	-0.01510	F_p,F_p	2138109.67415
D_c,Re	-0.62818	N_s,F_p	0.84183	σ,σ	-2138107.30478
P_l,N	-25.14590	N_s,A_{min}	1305031.66979	φ,φ	15.13155
P_l,S_h	-1.06816	N_s,A_o	-1305031.52873	D_h,D_h	-2138109.45007
P_l,N_s	1305031.45923	Re,Re	0.02156		

Table 4: *j* correlation

X,Y	**m**	**X,Y**	**m**	**X,Y**	**m**
2.7182, 2.7182	80532114.24837	P_l,D_h	3291518.00624	F_p,φ	196.46469
D_c,2.71828	272.23507	P_l,Re	-4808169.63015	F_p,D_h	-164.78005
P_l,2.71828	128165505.72604	P_l,$\eta_{estimator}$	-29101782.83246	F_p,$\eta_{estimator}$	4.25067
P_t,2.71828	149273733.15820	P_t,N	3291351.08118	A_{min},A_o	-3291546.72910
N,2.71828	135010031.64147	P_t,S_h	19673650.93865	A_{min},D_h	101.05339
S_h,2.71828	13636736.37394	P_t,N_s	1.94552	A_{min},Re	-4808172.76476
N_s,2.71828	3.63774	P_t,A_{min}	-62.41430	A_{min},$\eta_{estimator}$	-29101744.9640
F_p,2.71828	149274034.83714	P_t,A_o	195.62769	A_o,σ	-20.31916
A_{min},2.71828	-16545344.39966	P_t,Re	3.37499	A_o,D_h	3291513.23653
A_o,2.71828	-137291555.76133	P_t,$\eta_{estimator}$	-33.07601	A_o,Re	4808171.29008
σ,2.71828	149273936.13991	N,S_h	19673650.84243	A_o,$\eta_{estimator}$	29101779.03745
φ,2.71828	183.13149	N,F_p	3291547.75665	σ,φ	215.03115
D_h,2.71828	-132728584.19300	N,A_o	-6582830.21316	σ,D_h	-33.69463
Re,2.71828	-6665545.41733	N,σ	3291567.57427	φ,D_h	-205.12199
$\eta_{estimator}$,2.71828	-40343585.10246	N,φ	1.18293	φ,Re	-2.23851
D_c,N_s	-3.55960	N,D_h	-3291514.11156	D_h,Re	4808173.12570
D_c,F_p	318.77664	N,Re	-4808171.35908	D_h,$\eta_{estimator}$	29101743.36520
D_c,A_{min}	-11.42559	N,$\eta_{estimator}$	-29101779.87759	Re,$\eta_{estimator}$	0.52254
D_c,A_o	2.25004	S_h,F_p	19673651.42451	D_c,D_c	10.70934
D_c,σ	349.43770	S_h,A_o	-19673650.83474	P_l,P_l	-3291421.26901
D_c,D_h	-318.94552	S_h,σ	19673650.77249	N,N	3291415.78826
D_c,Re	-4.01888	S_h,D_h	-19673651.26124	F_p,F_p	62.45076
P_l,S_h	19673650.62038	N_s,F_p	5.91967	A_o,A_o	3291414.53865
P_l,N_s	1.60082	N_s,σ	5.04417	σ,σ	-55.78877
P_l,A_{min}	-3291476.73293	N_s,φ	-2.48344	φ,φ	-5.39275
P_l,φ	11.47026	N_s,D_h	-5.83856	Re,Re	0.03761
$\eta_{estimator}$,$\eta_{estimator}$	-1.89604				

Table 5: Slit Fin Correlation Summary

	ΔP	HTC
10% absolute deviation	98.1%	84.7%
15% absolute deviation	98.9%	93.2%
20% absolute deviation	100.0%	97.0%
Mean GCI[21*]	1.7%	1.3%

** Superscript 2 denotes baseline mesh and 1 denotes finer mesh*

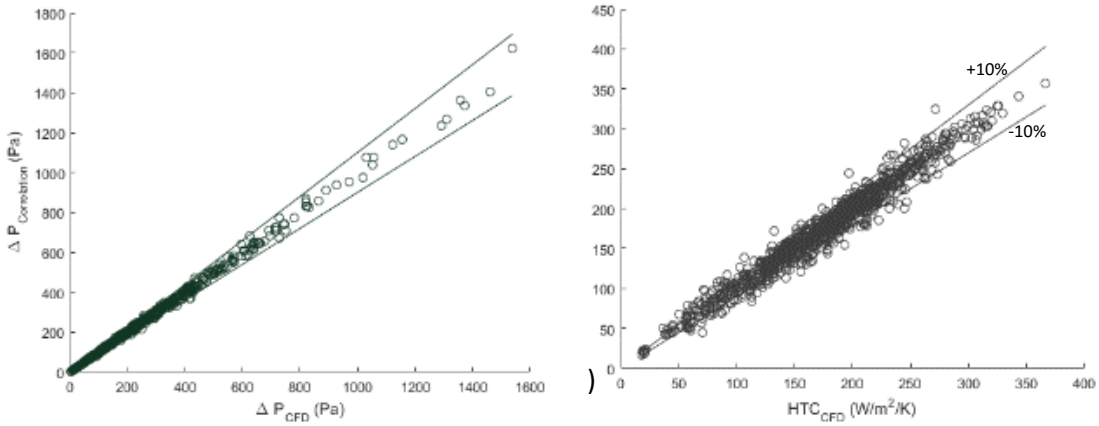

Figure 4: Verification of the correlations against the CFD data. (a) Pressure drop; (b) HTC

4. TREND ANALYSIS AND FIN OPTIMIZATION

The slit fin correlation developed in this work and the louver fin correlation developed by Sarpotdar et al. (2016) were used to conduct an analysis aiming to understand the influence of design variables such as the number of slits, number of louvers, etc. on fin performance. A multi-objective fin optimization study was also conducted to illustrate the capability to optimize a fin geometry for a particular set of objectives and constraints. Unless otherwise mentioned the design parameters for this study are as listed in Table 6.

Table 6: Design parameters of louver and slit fin used for comparison

Design Variable	Louver Fin	Slit Fin
D_n (mm)	4	4
C_l	3	3
C_t	1.5	1.5
N	2	2
N_s or N_l	4	3
FPI	27	27
u (m/s)	2.875	2.875
L_p (mm)	1.3	--
C_h	--	0.3 to 0.7

4.1 Trend Analysis

The following sections seek to find insights into the performance of these fin surfaces; the product of fin efficiency and HTC, ηHTC, is used as a metric for air-side heat transfer performance including the effect of fin efficiency. Figure 6 illustrates the influence of the number of louvers on the performance of a louver fin for ηHTC and the change in pressure drop. Note that for this study all variables except air velocity and the number of louvers were kept constant. Refer Table 6 to know the values of the design variables, e.g., C_l, C_t, FPI, etc., that are kept constant. As one can see in Figure 6, increasing the number of louvers increases both ηHTC and air pressure drop. Regardless of the air velocity, changing N_s from 2 to 8 increases ηHTC by about 30%. This is accompanied by an increase in pressure drop. In the high velocity range, the increase in pressure drop could be as much as 77%. The impact of the number of slits on the

fin slit fin performance is also illustrated in Figure 6. Changing the number for slits from 2 to 8 one can increase ηHTC by about 30 - 35%. This is accompanied by a pressure drop increase as high as 96%, in the high velocity range. Similar analysis was also done to assess the impact of louver pitch and slit height. It was found that both slit height and louver pitch have relatively low impact on ηHTC and pressure drop. For instance, changing the louver pitch from 0.8 mm to 1.8 mm does not change the ηHTC and pressure drop more than 12% and 23%, respectively. Changing slit height does not change the HTC and pressure drop more than 30% and 29%, respectively.

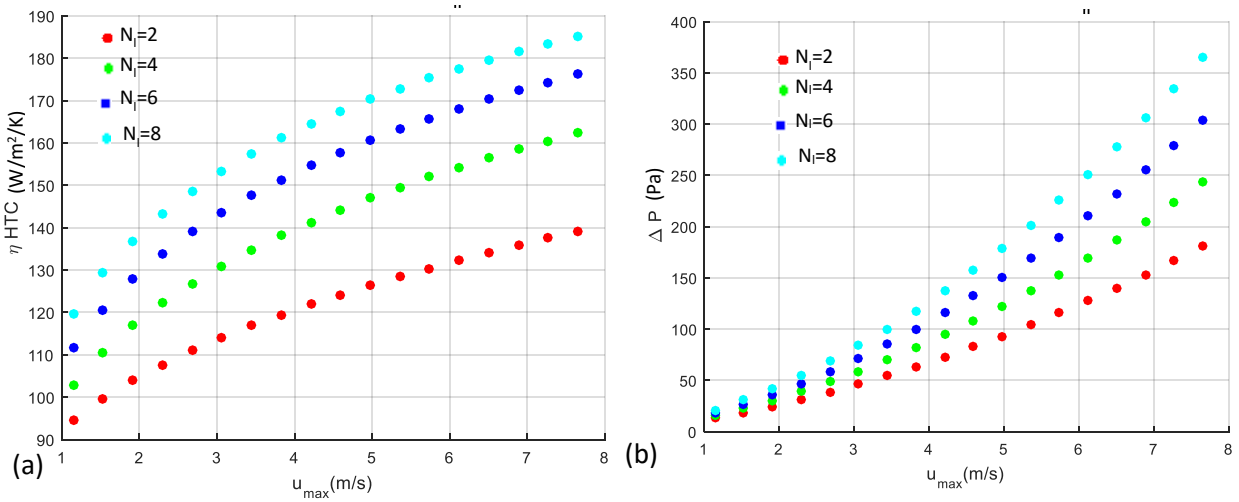

Figure 5: Influence of the number of louvers on (a) HTC and (b) pressure drop.

4.2 Fin Optimization

Selecting a fin design when all the design objectives and constraints are not known is challenging. A fin optimization study using a multi-objective genetic algorithm-based solver is shown here to illustrate a technique to identify optimal fin geometry parameters for a given scenario. The optimization study was performed for two different fins (slit and louver) and three (3 mm, 4 mm, 5 mm) different tube diameters with the objectives of maximizing ηHTC and minimizing pressure drop. In order to make sure there are no designs wherein slits or louvers intersect the tubes, appropriate manufacturing constraints are incorporated into the optimization problem, e.g., $P_l - (D_c - (2N_s - 1)S_w) > 0$ for slit fin and $P_l - (D_c - N_l L_p) > 0$ for louver fin. For this study, frontal air velocity, the number of tube banks, and fin density are fixed (refer to Table 6 for their respective values). Design parameters allowed to vary include C_l, C_t, L_p (C_h for slit fin), and N_l (N_s for slit fin). The lower and upper bounds for these design parameters are given in Table 7.

Figure 7 shows the results for slit fin optimization. Each subfigure shows three separate Pareto fronts, one for each of the three tube dimeters. Pareto fronts in each of these subfigures are shaded based on the value of the design variables such as C_l, C_t, etc. For instance, Pareto fronts in Figure 7a are shaded based on the value of the transverse pitch factor (C_t) of the individual design. In any of these subfigures, comparing the Pareto fronts for different tube diameters shows that smaller tube diameters result in higher ηHTC for any given pressure drop (ΔP). This indicates that the performance of the fin improves as the tube diameter reduces. Furthermore, reducing the transverse pitch factor (C_t) and/or increasing the number of slits (N_s), increases pressure drop as well as ηHTC (see Figure 7a and 7d, respectively). As long as the number of slits is kept constant, increasing C_h or reducing C_l increases pressure drop as well as ηHTC (see Fig. 7c and 7b respectively). It is to be noted that designs for this study varied Cl between 2 and 4. However, designs on the Pareto front show only values between a narrow range of 2 to 2.5. It should also be noted that despite a change in the number of slits, the Pareto fronts are relatively continuous. However, for louver fins, that is not the case. As one can see in Figure 8c, changing the number of louvers gives rise to a discontinuity, indicating substantial change in the performance of the louver fin. As long as the number of louvers are kept the same, increasing the louver pitch increases the pressure drop and ηHTC (Figure 8d). Comparing the Pareto fronts in Figures 7 and 8, it can be observed that performance of slit and louver fins is very comparable, except for the low pressure drop region. For instance, in Figure 8, one can see that 5 mm louver fin designs fail to produce a pressure less than 70 Pa. Whereas, 5 mm slit fin designs can result in a pressure drop as low as 57 Pa.

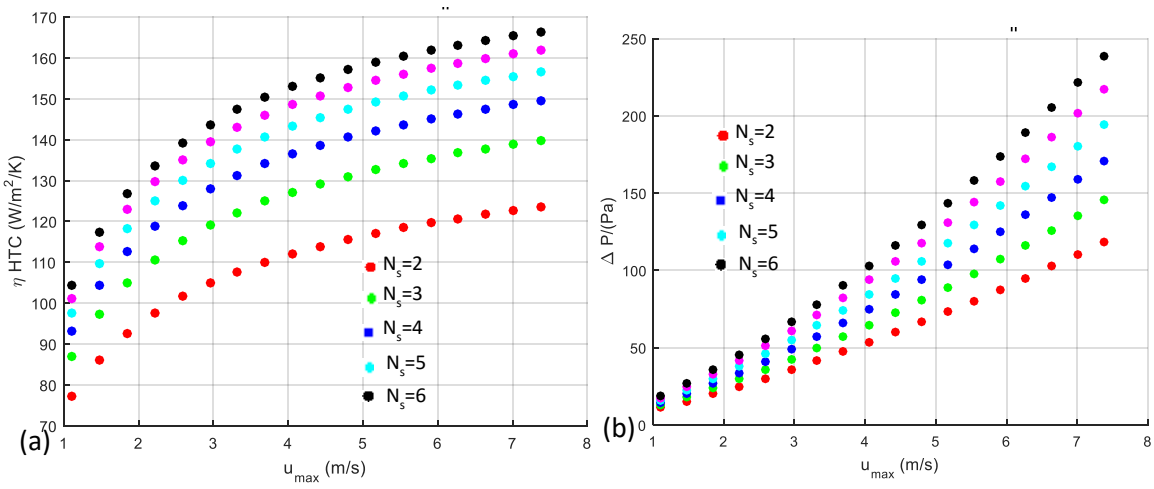

Figure 6: Influence of number of slits on (a) HTC and (b) pressure drop

Table 7: Range for various design parameters used in the fin optimization study

	C_l	C_t	N_s/ N_l	L_p/C_h
Louver	2 to 4	1 to 2	2 to 8	0.8 mm to 1.8 mm
Slit	2 to 4	1 1o 2	2 to 6	0.3 to 0.7

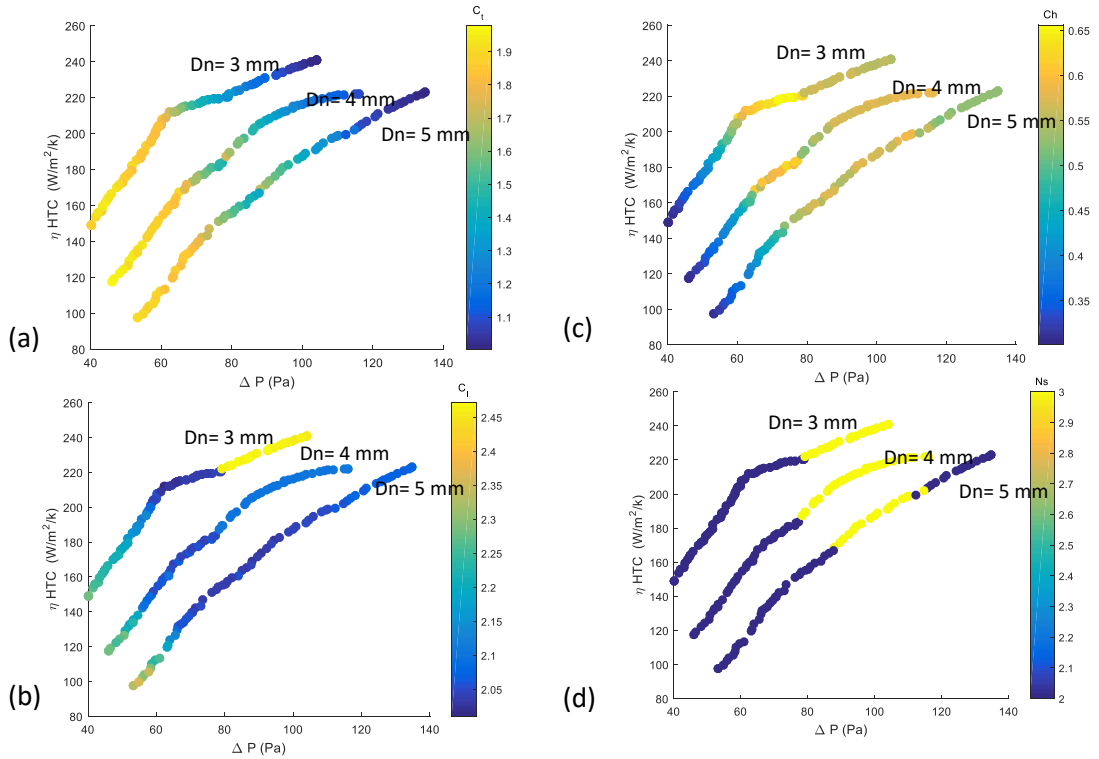

Figure 7: Pareto fronts for slit fin optimization study.

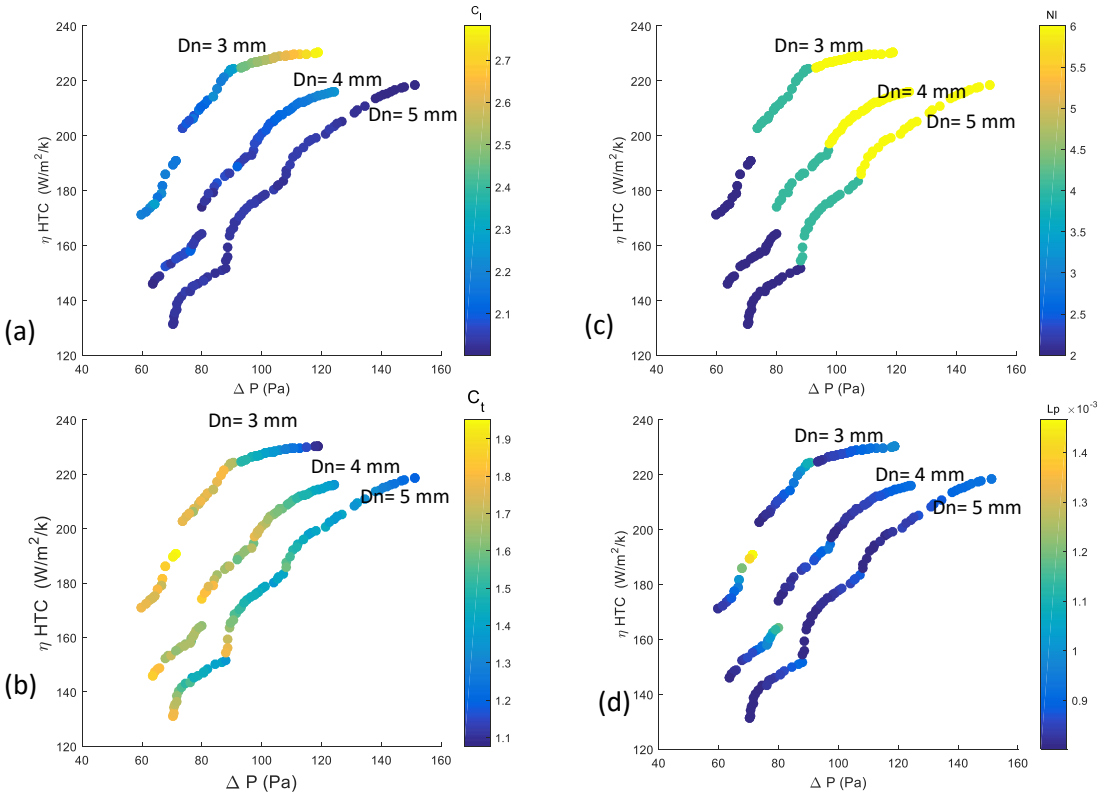

Figure 8: Pareto fronts for louver fin optimization study.

5. CONCLUSIONS

The present work develops airside pressure drop and HTC correlations for small diameter (3mm < D_n < 5mm) slit fins. These correlations are developed based on large data sets obtained from CFD simulations. The pressure drop correlation predicts 98% of the CFD data within 90% accuracy. The HTC correlation predicts 93% of the CFD data within 85% accuracy. This correlation along with the louver fin correlation developed by Sarpotdar et al. (2016) was used to study the influence of design parameters such as the number of slits, number of louvers, etc. on the performance of the fins. An effort is made to identify optimum fin designs for an illustrative example. The Pareto fronts from the optimization study show that slit and louver fins give comparable performance except when very low pressure drop is desired. For the fin optimization study considered in this study minimum pressure drop exhibited by the slit fins was lower than that of the louver fins. It is to be noted that the present fin correlations and fin design study is based on CFD simulations only. Work is underway to validate these correlations using physical heat exchanger testing.

NOMENCLATURE

A	area	(m^2)	L_p	Louver pitch	(m or mm)*
A_o	total (tube +fin) surface area	(m^2)	$\dot{m}$	mass flow rate	(kg/s)
cp	specific heat	(J/kg.K)	N_l/N_s	no. of louvers or slits	(-)
Dc	collar diameter	(m or mm)*	P	pressure	(Pa)
Di	inner tube diameter	(m or mm)*	Pr	Prandtl number	(-)
Do	outer tube diameter	(m or mm)*	P_t	transversal tube pitch	(m or mm)*
D_n	nominal tube diameter	(m or mm)*	P_l	longitudinal tube pitch	(m or mm)*
FPI	fins per inch	(-)	Q	heat rate	(W)
f	friction factor	(-)	Re	Reynold's no. ($\rho u_{max} D_c/\mu$)	(-)
G	mass flux	($kg/m^2.s$)	rg	mesh element size ratio	(-)

*Unless otherwise mentioned the unit is meter

h	heat transfer coefficient	(W/m².K)	S_h	slit height	(m or mm)*
h	mesh element size	(m or mm)*	T	temperature	(K)
j	colburn factor	(-)	u	velocity	(m/s)
k	thermal conductivity	(W/m.K)	UA_o	overall HTC	(W/K)

Greek letters

δ_f	fin thickness	(m or mm)*
μ	dynamic viscosity	(Pa·s)
η	fin efficiency	(-)
η_o	fin effectiveness	(-)
θ	louver angle	(degrees)
ρ	density	(kg/m³)
σ	contraction ratio	(-)
φ	fin efficiency geometrical parameter	(-)

Subscripts

f	fin
fr	frontal
m	mean
max	maximum
ref	refrigerant
w	wall

REFERENCES

ASME. (2009). Standard for Verification and Validation in Computational Fluid Dynamics and Heat Transfer – Section 2: Code verification, *ASME V&V 20 Standard*, 7-17.

Bacellar, D., Aute, V., Radermacher, R. (2014). CFD-Based correlation development for air side performance of finned and finless tube heat exchangers with small diameter tubes, *15th International Refrigeration and Air Conditioning Conference at Purdue University*, West Lafayette, Indiana, Paper 1410.

Paitoonsurikarn, S., Kasagi, N., Suzuki, Y. (2000). Optimal design of micro bare-tube heat exchanger, *Proceedings of the Symposium on Energy Engineering (SEE2000)*, vol. 3, pp. 972-979.

Roache, P. J. (1997). Quantification of uncertainty in computational fluid dynamics, *Annual Review of Fluid Mechanics*, 29, 123-160.

Saji, N., Nagai, S., Tsuchiya, K., Asakura, H., and Obata, M. (2001). Development of a compact laminar flow heat exchanger with stainless steel micro-tubes, *Physica*, C 354, pp. 148–51.

Sarpotdar, S., Nasuta, D., Aute, V., Radermacher, R. (2016). CFD-based airside heat transfer and pressure drop correlation development for small diameter (3 mm to 5 mm) louver fin heat exchangers, *16th International Refrigeration and Air Conditioning Conference at Purdue University*, West Lafayette, Indiana, Paper 2363.

Schmidt, T. E. (1949). Heat transfer calculations for extended surfaces, *Refrigerating Engineering*, Vol. 57, pp. 351-357

Wang, C., Chi, K. (2000). Heat transfer and friction characteristics of plain fin-and-tube heat exchangers, part I: new experimental data, *International Journal of Heat and Mass Transfer*, 43, 2681-2691.

Webb, R.L., Kim, N., 2005, Principles of Enhanced Heat Transfer, New York: Taylor & Francis, Ch. 2, pp. 1-32

ACKNOWLEDGEMENT

The present work was supported by the International Copper Association. Authors acknowledge Hal Stillman from the International Copper Association, Yoram Shabtay from Heat Transfer Technologies, LLC and Roger Tetzloff from Burr Oak Tool for their valuable comments.